Plasmonics (2022) 17:1387–1402
https://doi.org/10.1007/s11468-022-01622-x

Antibacterial, Cytotoxic, and Catalytic Potential of Aqueous *Amaranthus tricolor*–Mediated Green Gold Nanoparticles

Mamatha Susan Punnoose[1] · Siby Joseph[2] · Bony K. John[1] · Anu Rose Chacko[1] · Sneha Mathew[1] · Beena Mathew[1]

Received: 16 November 2021 / Accepted: 22 March 2022 / Published online: 4 April 2022

Abstract

This article reports an unexploited method for the green synthesis of gold nanoparticles using *Amaranthus tricolor* leaves, with the aid of microwave assistance. The fresh leaf extract of the plant plays dual role in reducing and capping actions. The incorporation of microwave energy to this green approach overcomes the characteristic limitation of time consumption by the conventional green techniques. The synthesized gold nanoparticles are characterized using UV–vis., FT-IR, XRD, HR-TEM, EDX, DLS, and zeta potential analyses. The various functional groups in the plant extract which are responsible for the reduction and stabilization of nanoparticles were identified by FT-IR spectrum. The crystallographic peaks designated to face centered cubic lattice of the gold nanoparticles are evident from the XRD analysis. HR-TEM images illustrate the almost spherical morphology attained by the formed nanoparticles with an average particle diameter of 18.33 nm. The stability of nanoparticles is revealed by its zeta potential of − 21.3 mV. The DLS analysis results in a hydrodynamic diameter of 148.5 nm. The catalytic potential of the synthesized gold nanoparticles in the attenuation of harmful pollutants such as eosin Y and 2-nitrophenol by $NaBH_4$ was studied. Both the catalytic degradations were successfully completed within few minutes of the reaction and they hold to pseudo-first order kinetics. The nanoparticles accomplished good antibacterial properties towards various bacteria and are demonstrated herein. Cytotoxic activity of the synthesized nanoparticles was evaluated for human lung cancer cell line A549 using MTT assay and a LC_{50} value of 102.39 ± 0.36 µg/mL was obtained.

Keywords Green synthesis · Gold nanoparticles · *Amaranthus tricolor* · Catalytic degradation · 2-nitrophenol · Eosin Y

Introduction

Metal nanoparticles have emerged as a new avenue of opportunities and novel applications in the field of nanotechnology due to their unique properties which vastly differ from their bulk counterparts. Among the different noble metal nanoparticles, gold nanoparticles are gaining a lot of significance in the recent years because of their enticing applications in the catalysis, biomedical, drug delivery, sensing, optics, and imaging [1–3]. The utilization of gold nanoparticles as both homogenous and heterogenous catalyst in various reactions is clearly evident in their key applications [4–6]. This high catalytic potential is attributed towards their physico-chemical properties due to the small particle size, morphology, quantum confinement, and large surface area [7].

The synthesis of metal nanoparticles can be achieved by means of chemical, sonochemical, photochemical, microemulsion, radiolytic, and microwave techniques [8–10]. Upon environmental concerns and focus on green chemistry, the strategy of microwave synthesis is the frequently adopted method. Microwave irradiation provides uniform heating, homogenous nucleation, and requisite growth conditions for the nanoparticle production within very short reaction time [11]. Overall, the procedure is fast, cost-effective, clean, and ecofriendly. Energy transfer from microwave radiation to the reactants is achieved by the interaction of the radiation with water or other high dielectric constant solvents or solvent molecules with large dipole moments [12]. Based on the ease of natural availability, simplicity, and safety in handling, plant extracts are the mostly preferred non-chemical reducing and stabilizing agent than other biological entities like natural products, biopolymers, or microorganisms. The

✉ Beena Mathew
beenamathew@mgu.ac.in

[1] School of Chemical Sciences, Mahatma Gandhi University, Kottayam 686560, Kerala, India

[2] Department of Chemistry, St. George's College, Aruvithura, Kottayam 686122, Kerala, India

incorporation of microwaves to this approach offers a simple route for the preparation of gold nanoparticles, which results in the successful completion of reaction with better yield of products involving lower energy utilization [13]. Moreover, this methodology precludes the use of toxic chemicals and coarse reaction requirements which were fundamental in the traditional means. The disadvantage of requiring longer reaction times for biological means to produce nanoparticles is mitigated by the action of unconventional microwave strategies and does not interfere with the required green reaction conditions [14, 15]. Green synthesis of gold nanoparticles using different plants including *Euphorbia tirucalli* [16], *Aerva lanata* [17], and *Garcinia kola* [18] with the aid of microwave energy is reported.

Recently, environmental issues regarding fresh water contamination and shortage of adequate drinking water are increasing consideration everywhere throughout the world. The disposal of untreated industrial effluents and domestic wastage into the natural aquatic environment is of global concern. Vital toxic pollutants mainly include synthetic dyes and more than 100,000 different dyes are produced annually [19]. Dyes are class of organic compounds which find extensive use in paper, leather, glass, textiles, cosmetics, ceramics, and pharmaceutical industries [20]. Their ability to impart color into the medium even at mild concentrations makes them a major contaminant in the waste water effluents. They are potent carcinogen, mutagen, eye, and skin irritant and may cause major health hazards upon inhalation or ingestion [21].

Aromatic nitro compounds are another set of hazardous organic pollutants which are a major threat to the water environment. They are produced from different industrial and agriculture processes including the manufacture of herbicides, pesticides, synthetic dyes, explosives, drugs, and other products [22]. They dangerously affect the human reproductive and central nervous systems [23]. The stability, water solubility, and inhibitory nature of nitroaromatics adulate their toxicity.

Besides human health problems, the discharge of organic contaminants into the water sources causes deprivation of oxygen in fresh water streams, decreases sunlight penetration, and thereby affects the aquatic life [24]. Thus, alleviation of these anthropogenic pollutants in the waste water becomes a prerequisite to their disposal. The high chemical stability and microbial resistance of these pollutants obturate the conventional water treatment methods like biodegradation, adsorption, and ultrafiltration to become effectual [25]. Latest reports suggest that catalytic activity of green nanomaterials has been expanded to the sector of waste water treatment also [14, 15]. From the ecological point of view, the development of such an effective and facile method for the abatement of organic pollutants from waste water is significantly adorable.

In this paper, we report a novel microwave-assisted green synthesis of gold nanoparticles using aqueous extract *Amaranthus tricolor* as the reducing and stabilization agent. *Amaranthus tricolor* is a medicinal plant which belongs to the family of *Amaranthaceae*. They are used in the treatment of piles, bronchitis, leucorrhoea, blood disorders, and even as laxative, stomachic, diuretic, hemorrhage, antipyretic, and hepatoprotective agent [26]. Amaranthin is the main betacyanin violet pigment in the plant [27]. The phytochemical analysis of its aqueous extract shows the presence of alkaloids, tannins, flavonoids, saponins, amino acids, proteins, and phenolic compounds [28]. Microwave heating aids in the complete reduction of Au^{3+} to Au^{0} within 1 min. The *Amaranthus tricolor*–mediated gold nanoparticles (AuNP-AT) are characterized using UV–vis., FT-IR, HR-TEM, EDX, DLS, and zeta potential analyses. The prospective catalytic efficiency of AuNP-AT is examined for reductions of 2-nitrophenol and eosin Y. Also, the cytotoxic and antibacterial properties of the nanoparticles were also evaluated.

Experimental

Materials

All the chemicals purchased were of analytical grade and were used as such with no further purging. Hydrogen tetrachloroaurate (III) trihydrate ($HAuCl_4.3H_2O$, 99.99%) was purchased from Sigma-Aldrich. Eosin Y (99%), 2-nitrophenol (98%), and sodium borohydride (98%) were obtained from Merck. All solutions were prepared using double distilled water in the entire experiment. Fresh leaves of *Amaranthus tricolor* were identified and collected.

Methods

Preparation of *Amaranthus tricolor* (AT) Leaf Extract

About 25 g of the leaves of *Amaranthus tricolor* was chopped into fine pieces and boiled for 1 h with 100 mL distilled water. The aqueous extract is filtered and stored at 4 °C for further studies.

Green Synthesis of Gold Nanoparticles Using *Amaranthus tricolor* Leaf Extract (AuNP-AT)

Amaranthus tricolor (AT) leaf extract and 1 mM solution of the gold salt were mixed in a 250-mL beaker in a specific ratio. It was then subjected to microwave irradiation for 60 s in a domestic microwave oven (Sharp R-219 T(W)), 2450 MHz). The reduction of Au^{3+} to Au^{0} was visually identified by the color change of the reaction mixture from pale pink to violet. Confirmation on the formation of gold

nanoparticles was done by monitoring the UV–vis absorption spectrum in the range of 200–800 nm. The optimization by means of composition ratio of AT extract to the gold salt, microwave irradiation time, and power was also investigated.

Catalytic Studies

The catalytic reduction of eosin Y (1×10^{-4} M) and 2-nitro phenol (4×10^{-4} M) was studied. It involves the mixing of 2.5 mL of the organic pollutant, cold solution of 0.5 mL freshly prepared $NaBH_4$ (0.6 M), and 0.25 mL AuNP-AT in a quartz cuvette of 1 cm path length. The degradation of both pollutants was identified by its solution decolorization and were monitored using UV–vis spectrophotometer in the range of 200–800 nm at regular intervals of time.

In Vitro Cytotoxic Studies Using MTT Assay

The cytotoxic effect of *Amaranthus tricolor* (AT) leaf extract and AuNP-AT against A549 (Human Lung cancer) cells was determined using MTT (3-(4, 5-dimethylthiazol-2-yl)-2,5-diphenyltetrazolium bromide) assay. The cell lines were procured from National Centre for Cell Sciences (NCCS), Pune, India, and was maintained in Dulbecco's modified Eagles medium (DMEM) supplemented with 10% FBS, L-glutamine, sodium bicarbonate (Merck, Germany), and antibiotic solution containing the following: penicillin (100U/mL), streptomycin (100 µg/mL), and amphoteracin B (2.5 µg/mL). Two-day-old confluent monolayer of cells was trypsinized and the cells were suspended in 10% growth medium, and 100 µL cell suspension (5×10^3 cells/well) was seeded in 96-well tissue culture plate. The cultured cell lines were kept at 37 °C in a humidified 5% CO_2 incubator (NBS Eppendorf, Germany). The viability of cells was evaluated by direct observation of cells by inverted phase contrast microscope and followed by MTT assay method.

Various amounts of the plant extract and gold nanoparticles (6.25, 12.5, 25, 50, and 100 µg/mL) were added to the grown cells and were incubated for 24 h. The untreated cells serve as the control. After incubation period, entire plates were observed using inverted phase contrast tissue culture microscope (Olympus CKX41 with Optika Pro5 CCD camera) and microscopic observation was recorded as images.

After 24 h of incubation period, the sample content in wells was removed and 30 µL of reconstituted MTT solution was added to all test and cell control wells, and the plate was gently shaken well, then incubated for 4 h (at 37 °C in 5% CO_2 incubator). After the incubation period, the supernatant was removed and 100 µL of MTT solubilization solution (dimethyl sulphoxide, DMSO, Sigma-Aldrich, USA) was added and the wells were mixed gently by pipetting up and down in order to solubilize the formazan crystals. The absorbance values were measured by using microplate reader at a wavelength of 540 nm. The whole experiment is done in triplicate. The percentage of cell viability was calculated using the following equation.

$$\%\ cell\ viability = \frac{Mean\ OD\ of\ Samples}{Mean\ OD\ of\ control} \times 100$$

where "OD" stands for optical density. The LC_{50} values were calculated using ED50 PLUS V1.0 software and mean ± standard deviation was also identified.

Antibacterial Studies

The potential of synthesized gold nanoparticles as antibacterial agents was accessed by using the agar well diffusion method. Petriplates containing 20 mL Muller Hinton agar medium were seeded with bacterial culture of *Escherichia coli*, *Pseudomonas aeruginosa*, *Streptococcus mutans*, and *Staphylococcus aureus*. Wells of approximately 10 mm were bored using a well cutter and 100 µL of the samples was added. The plates were then incubated at 37 °C for 24 h. The antibacterial activity was assayed by measuring the diameter (in mm) of the inhibition zone formed around the well and distilled water was used as the control.

Characterization Techniques

The green-synthesized AuNP-AT was characterized by Shimadzu UV-2450 spectrophotometer (UV–vis spectra), Perkin Elmer-400 FT-IR spectrometer (FT-IR spectra), Bruker AXS D8 Advance X-ray diffractometer (XRD diffractions), JEOL-2100 model microscope (HR-TEM and EDX) and Horiba SZ-100 scientific nanoparticle analyzer (DLS and zeta potential).

Results and Discussion

UV–vis Spectroscopy

The aqueous extract of AT acts as both a reducing and capping agent for the synthesis of AuNP-AT. The microwave-assisted gold nanoparticles synthesis was monitored using UV–vis spectroscopic technique in the range of 200–800 nm. The green-synthesized AuNP-AT was primarily identified by the color change of the solution mixture from pale pink to violet upon 1 min of microwave heating. It was confirmed by the absorbance band at 534 nm which corresponds to the surface plasmon resonance (SPR) in the UV–vis spectrum (Fig. 1). Also, the AT extract did not show any peak in this range.

In the phytomediated synthesis, formation and nucleation of gold nanoparticles were resulted by the transfer of charge

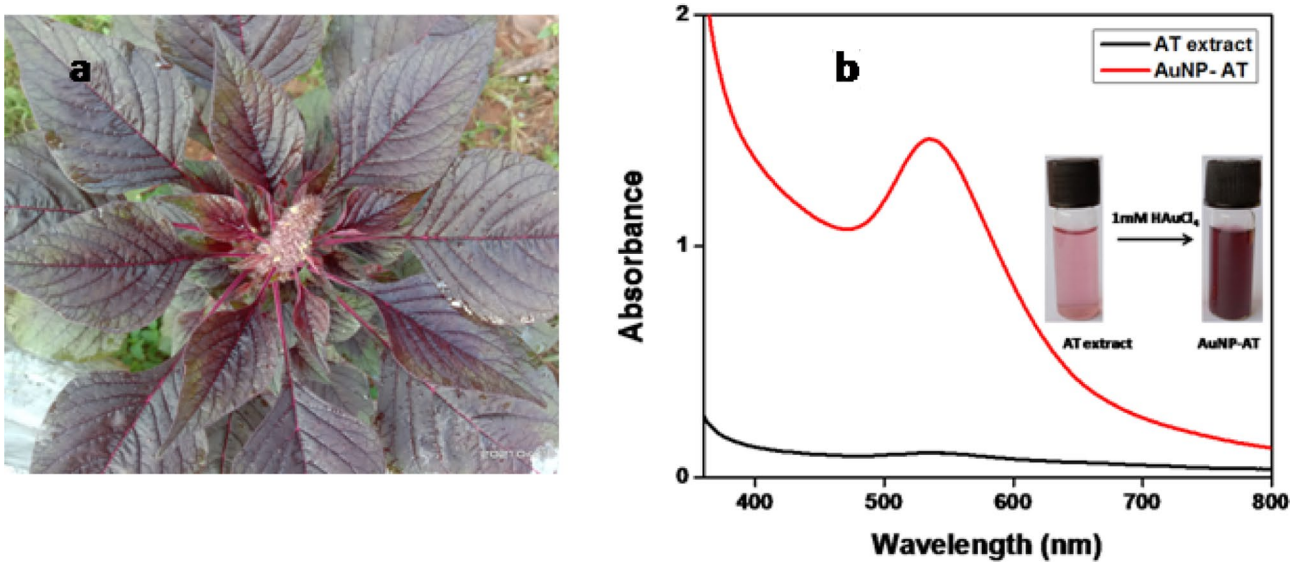

Fig. 1 **a** Photograph of *Amaranthus tricolor* and **b** UV–vis spectra of AT extract and AuNP-AT

from the various biomolecules in the plant extract such as proteins, amino acids, enzymes, flavonoids, and terpenoids to Au^{3+} ions. While few molecules of phytochemicals get adsorbed on the nanoparticles surface by means of coulombic forces of attraction and form electrostatic double layers [29]. Due to the van der Walls forces of attraction, a diffuse double layer was formed around this electrostatic double layer through adsorption of various layers of phytochemicals. Electrostatic or steric barriers take place around the surface of gold nanoparticles due to the variations in the molecular structures of phytochemicals present in the AT extract. This led to the effective capping of the synthesized nanoparticles by restricting its agglomeration and enhancing their stability.

The green synthesis of AuNP-AT was optimized by varying the compositional ratio between AT extract and gold salt, microwave irradiation power, and irradiation time. Different compositions of AT extract and tetra chloroaurate solution were tried for the green synthesis of AuNP-ATas shown in Fig. 2a. For 1:3 ratio, nanoparticle formation did not occur. In case of 1:5 ratio, the formation of nanoparticles was identified but the absorption band was not sharp enough. A broadened peak appeared in 1:7 composition. While 1:9 composition exhibited a smooth sharp peak at 534 nm in the absorbance spectrum which manifests the monodispersitivity of the formed AuNP-AT particles. Thus, this 1:9 is well chosen over other ratios for further studies.

The effect of microwave power on the AuNP-AT synthesis using 1:9 composition was studied between 200 and 800 W, by maintaining the time of irradiation a constant (Fig. 2b). The formation of nanoparticles was not initiated at 200 W. Out of the various smooth absorbance bands obtained for 400, 600, and 800 W of AuNP-AT synthesis, the most intense and sharp one was that of 800 W (Fig. 2b). The optimum irradiation power was thus fixed at a power of 800 W.

The dependance of microwave irradiation time on AuNP-AT synthesis was monitored at every 15 s of heating. An increase in the absorbance of the SPR band around 534 nm with irradiation time was observed and reached a maximum within 60 s (Fig. 2c). No considerable change in the position and absorbance of the peak was detected even after 1 min of microwave heating due to the absence of nanoparticle agglomeration.

FT-IR Spectra

FT-IR analysis helps in the identification of various functional groups present in the plant extract which are responsible for the reduction of gold salt. Figure 3 shows the FT-IR spectra of AT extract and AuNP-AT. A strong absorption band at 3371 cm^{-1} corresponds to the stretching vibration of -O–H bond. The bands at 2949, 1625, 1225, and 1090 cm^{-1} are due to the aliphatic C-H, -C = O, C-O, and C–O–C stretching vibrations of different phytochemicals present in the AT extract [30]. Bands at 1388 and 1016 cm^{-1} confirmed the presence of aromatic and aliphatic amines, respectively [31]. Thus, the hydroxyl, carboxyl, and amine groups played an important role in both reduction and stabilization process of the synthesized AuNP-AT. A slight displacement in peak positions of AT extract is observed in AuNP-AT.

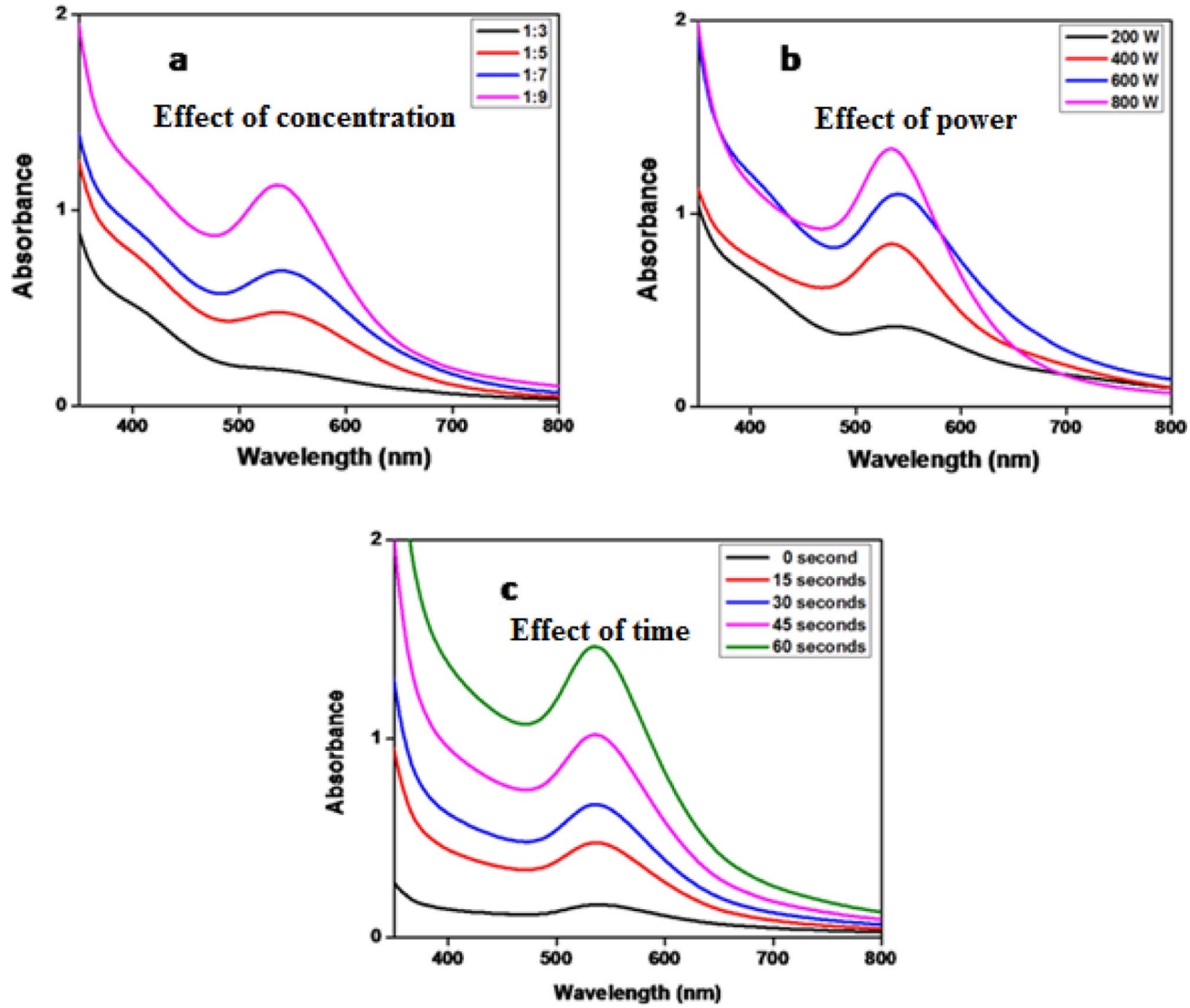

Fig. 2 UV–vis spectra showing the effect of **a** compositional ratio between AT extract and $HAuCl_4$ where 1:9 is optimum, **b** microwave power level where 800 W is optimum, and **c** microwave irradiation time where 60 s is optimum for the formation of AuNP-AT

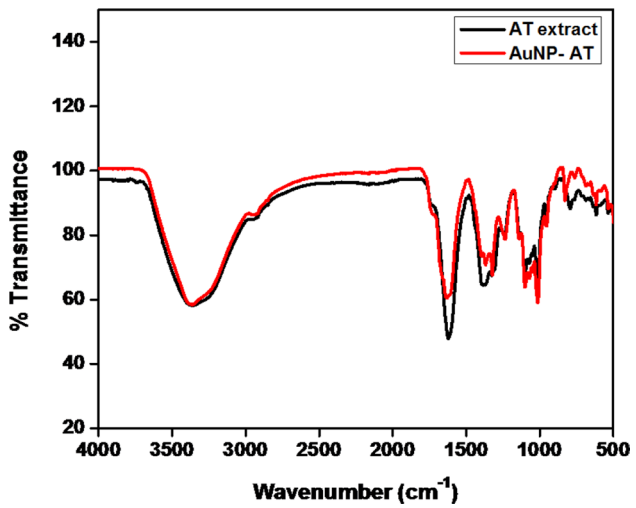

Fig. 3 FT-IR spectra of **a** *Amaranthus tricolor* extract, and **b** AuNP-AT

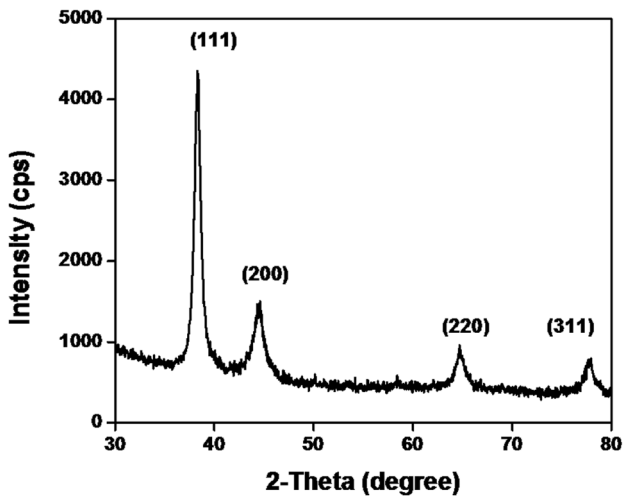

Fig. 4 XRD pattern of AuNP-AT

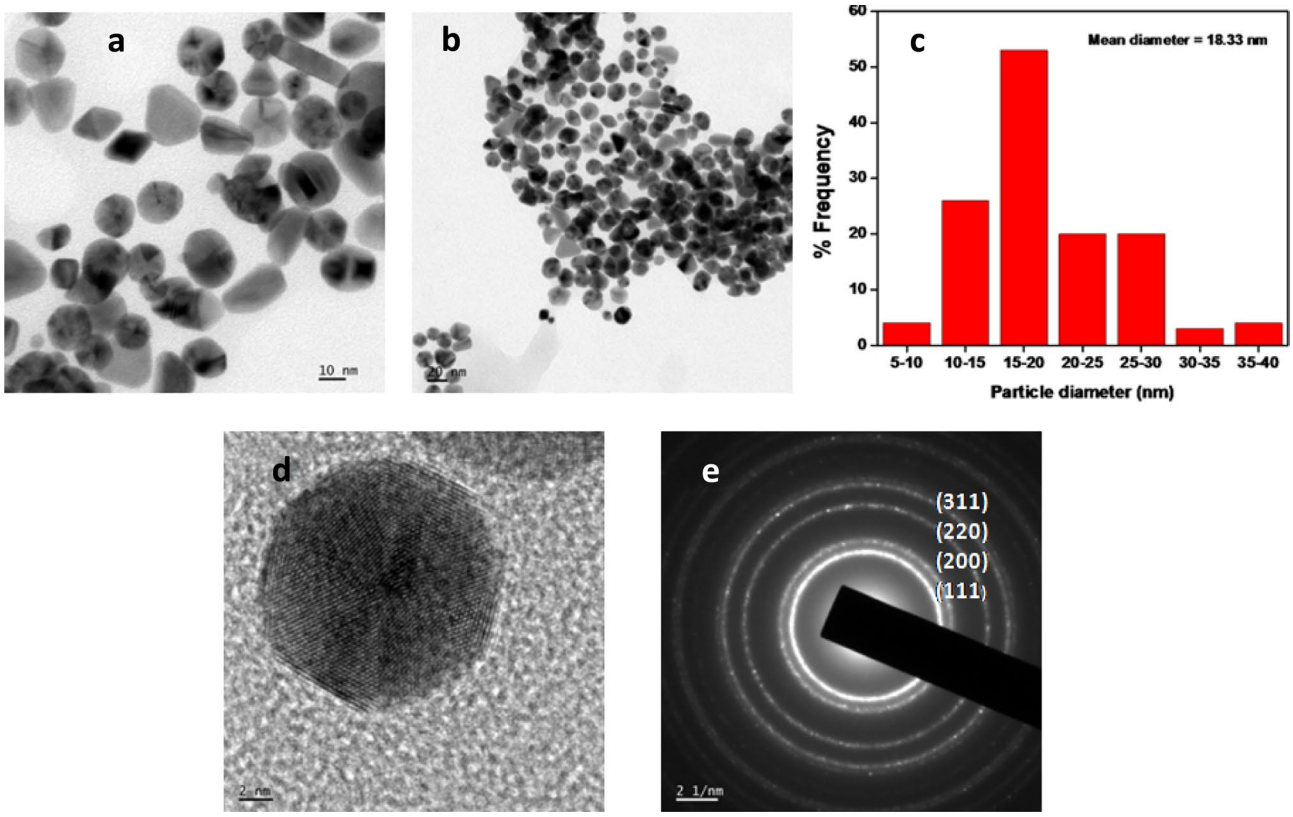

Fig. 5. **a** and **b** TEM images of AuNP-MF at different magnifications, **c** particle-size histogram, **d** HR-TEM image, and **e** SAED pattern of the formed AuNP-AT

XRD Analysis

The XRD pattern aids in determining the highly crystalline nature of the formed AuNP-AT. The highly distinct and intense diffraction patterns at 2θ values of 38.31°, 44.41°, 64.61°, and 77.82° matches the reflections from (111), (200), (220), and (311) planes of face-centered cubic lattice of metallic gold nanoparticles (Fig. 4). These values are much similar to that of JCPDS file no. 04–0784 [32]. Out of the four diffraction peaks, the one which corresponds to the (111) plane is the more preferred plane of orientation by the AuNP-AT.

Fig. 6 EDX spectrum of AuNP-AT

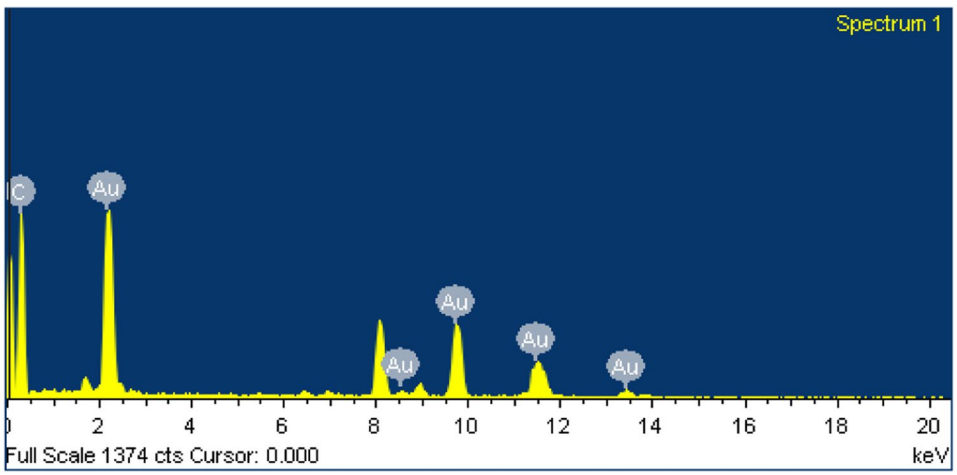

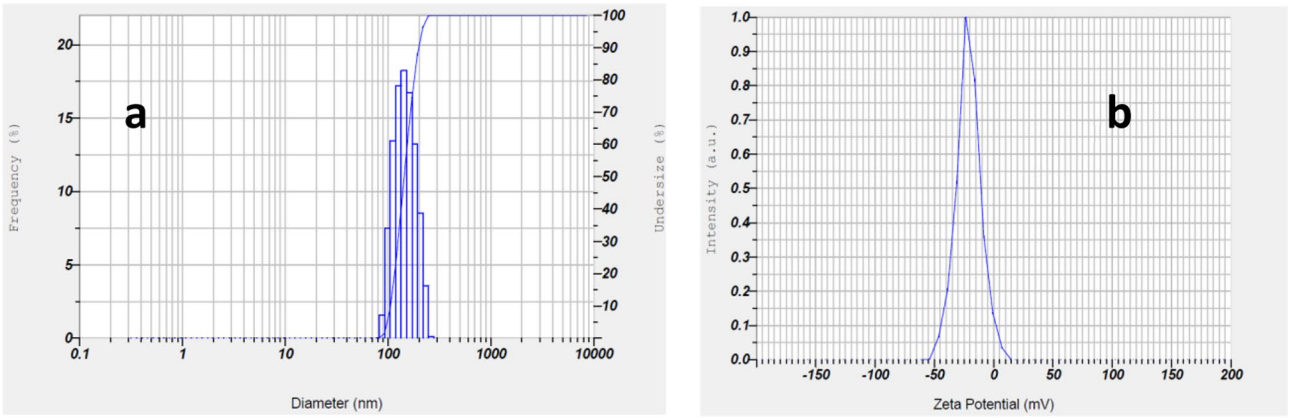

Fig. 7 **a** DLS and **b** zeta potential measurement of AuNP-AT

HR-TEM and SAED Analysis

The TEM micrographs at different magnifications of the synthesized AuNP-AT are depicted in Fig. 5a and b. The polydispersive nature of the gold nanoparticles is simply evident from the various morphologies adopted such as triangular plate, spherical, and rod shapes. Majority among them are of almost spherical morphology and the average diameter of particles is found to be 18.33 nm (Fig. 5c). The HR-TEM image of the formed AuNP-AT shows the clear lattice fringes (Fig. 5e). Bright circular rings in the selected area diffraction (SAED) pattern validate the pure crystallinity of the nanoparticles. The SAED fringes in Fig. 5d correspond to the (111), (200), (220), and (311) planes of the face-centered gold which are in good agreement with the XRD pattern.

EDX Analysis

The EDX analysis of AuNP-AT showed signals at 2.3, 8.2, 9.8, 11.5, and 13.4 keV, which confirms the presence of elemental gold (Fig. 6). The sharp signals indicated the complete reduction of gold ions to elemental gold. Signals of carbon may arise from the phytochemical constituents in the leaf extract of AT.

DLS and Zeta Potential Measurements

The particle size obtained from the DLS analysis is found to be 148.5 nm which is much larger than their TEM results (Fig. 7a). This is so because in TEM, individual particle diameter is determined. While DLS measures the intensity of the scattered light from the core nanoparticles and the

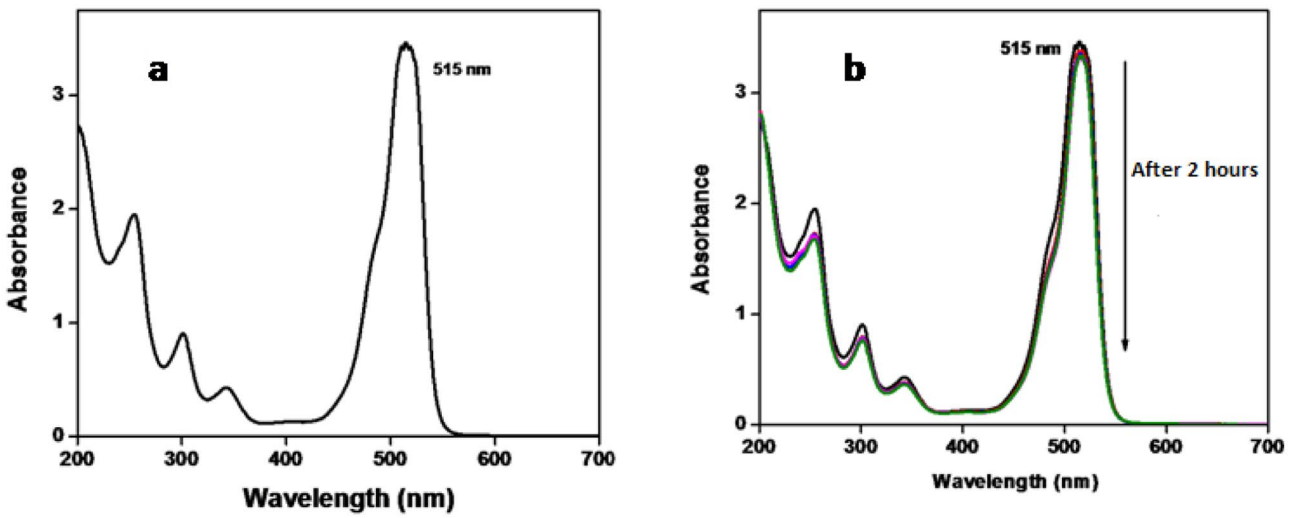

Fig. 8 UV–vis spectra of **a** eosin Y, and **b** degradation of eosin Y in the presence of $NaBH_4$ alone

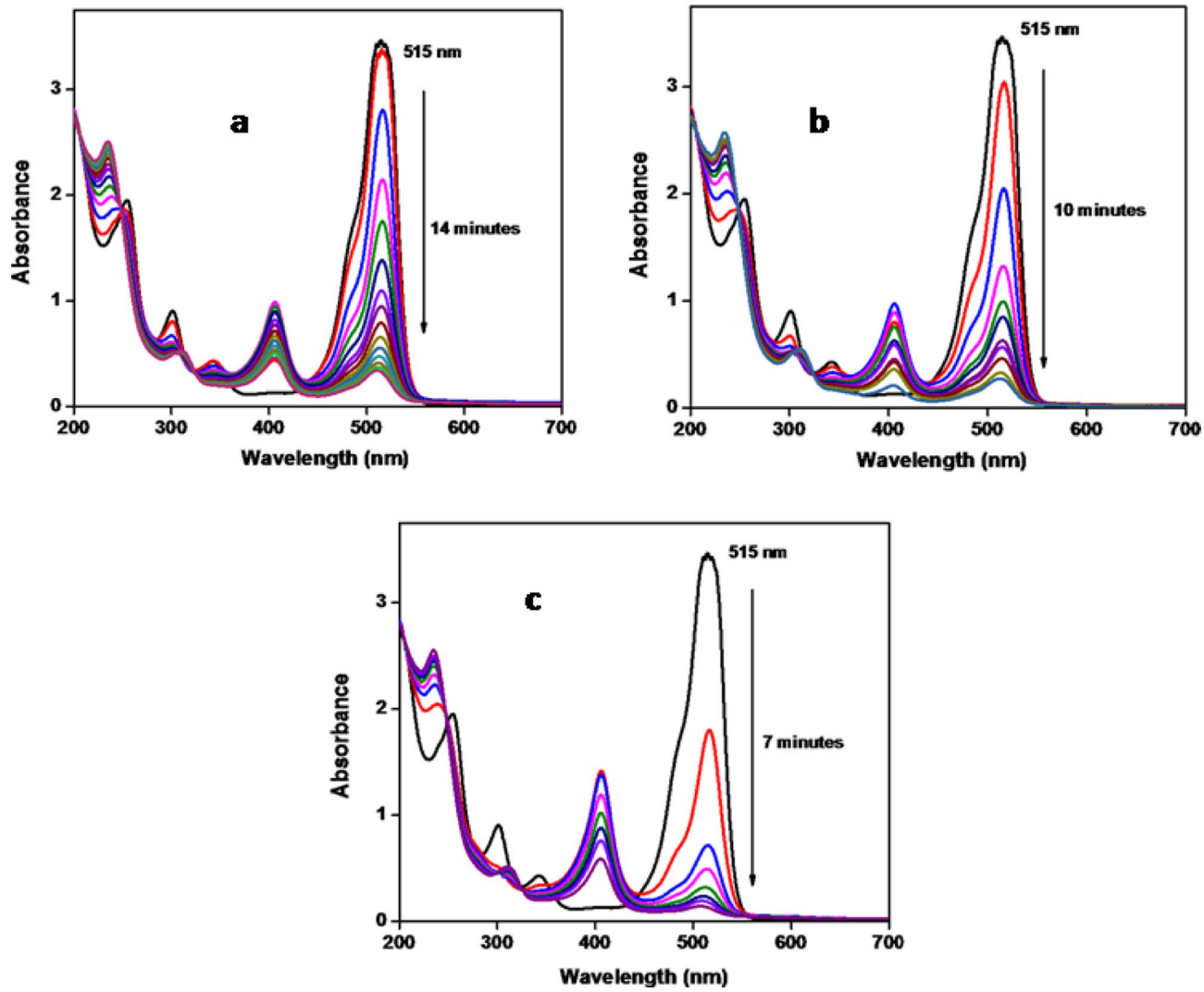

Fig. 9 UV–vis absorption spectra for the degradation of eosin Y by $NaBH_4$ in presence of **a** 0.02, **b** 0.03, and **c** 0.04 mg/mL concentration of AuNP-AT catalyst

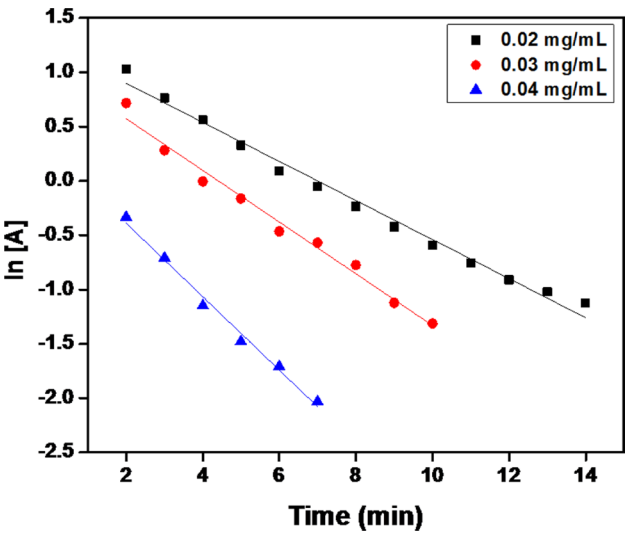

Fig. 10 Plot of *ln* [*A*] against time for the reduction of eosin Y

phytochemical cloud around the gold nanocore is analyzed as a function of time and thus the hydrodynamic size of nanoparticles is determined. The effect of Brownian motion and size measurement using Stokes–Einstein relationship is of much importance in DLS analysis. Thus, the nanoparticle measured size is somewhat larger than the actual size measured from TEM analysis. The zeta potential value

Table 1 Catalytic activity of AuNP-AT in the reduction of eosin Y

Concentration of AuNP-AT ($mgmL^{-1}$)	Time (min)	Rate constant k (min^{-1})	Correlation coefficient (R^2)
0.02	14	0.1797	0.9882
0.03	10	0.2379	0.9827
0.04	7	0.3377	0.9880

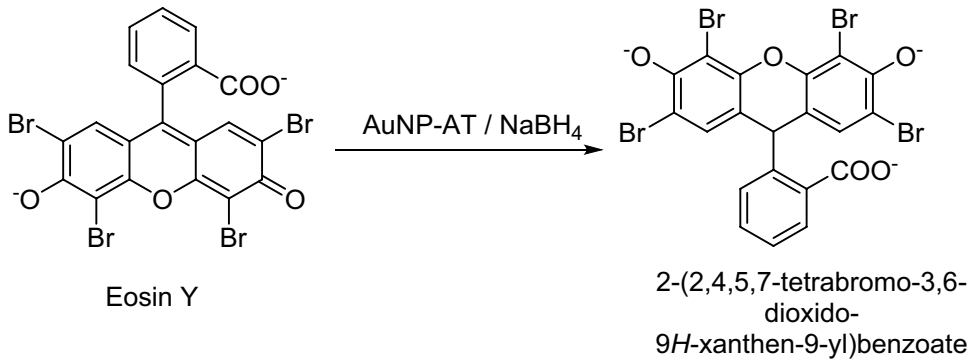

Fig. 11 Schematic representation for the reduction of eosin Y

of − 21.3 mV for AuNP-AT particles confirms its stability (Fig. 7b). The DLS and zeta potential measurements were carried out at an instrumental controlled setup of 25 °C.

Catalytic Reduction of Eosin Y

Eosin Y is a water soluble heterocyclic dye having four bromine atoms, which belongs to the xanthene family. They are used in fluorescent pigments, histological staining, textile, and leather industries [33, 34]. The direct discharge of eosin Y into water streams is a serious threat to the environment due to its dark orange color, toxicity, and high stability because of their complex aromatic structure [35, 36].

The absorption spectrum of eosin Y shows a prominent peak at 515 nm (Fig. 8a). The UV–vis spectra of the dye with $NaBH_4$, in the absence of AuNP-AT catalyst, did not show a much appreciable change in their absorbance as well as in the orange color of its aqueous solution even after several hours of the reaction (Fig. 8b). Upon the addition of 0.02 mg/mL AuNP-AT catalyst, a progressive reduction of the dye initiated and the reaction was completed within 14 min (Fig. 9a). The completion of catalyst-supported dye reduction was identified by the visual color change from orange to colorless. This shows that the degradation is not effectual in the absence of gold catalyst or in the presence of reducing agent, $NaBH_4$ alone. The UV–vis spectra at 515 nm were monitored at every 1-min interval during the course of the degradation.

Metal nanoparticles accelerate the degradation process by means of their electron relay between the donor–acceptor molecules. The large surface area availability and intermediate reduction potential of the gold nano catalyst between the borohydride (donor) and dye (acceptor) moieties contribute towards their catalytic activity. The reduction mechanism involves the effective adsorption of both reactants, dye and borohydride ions, onto the surface of AuNP-AT catalyst and efficient electron transfer between them [37]. The phytoconstituents surrounding the metal nanoparticles aid in bringing the reactant groups in a closer proximity to the catalyst surface by means of electrostatic interactions. Thus, a kinetically forbidden reaction becomes an allowed one.

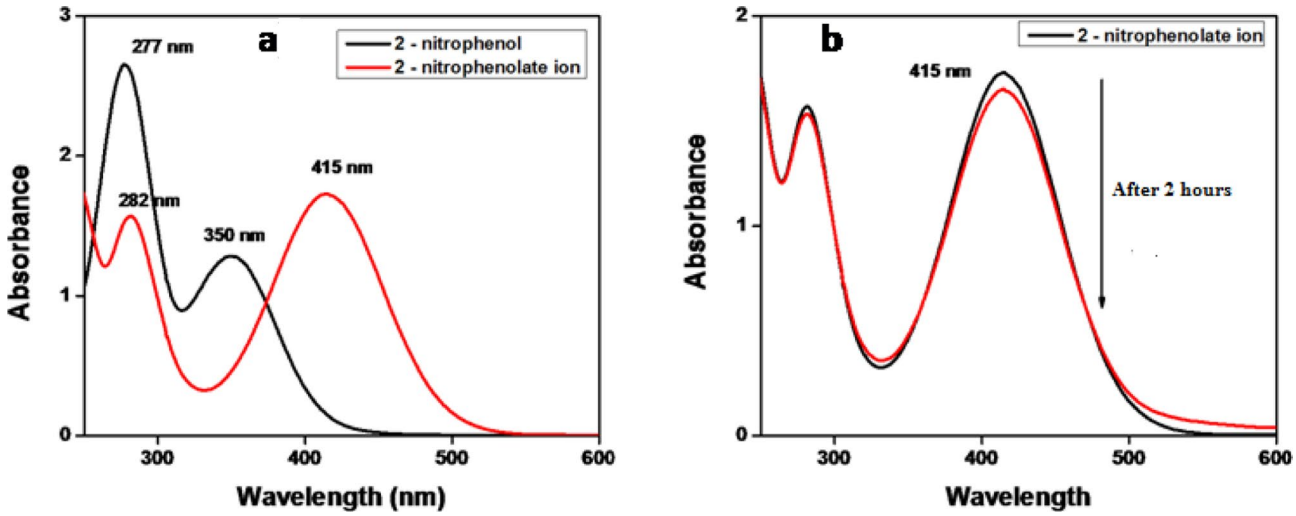

Fig. 12 UV–vis spectra of **a** 2-nitrophenol and 2-nitrophenolate ion, and **b** reduction of 2-nitrophenol by $NaBH_4$ alone

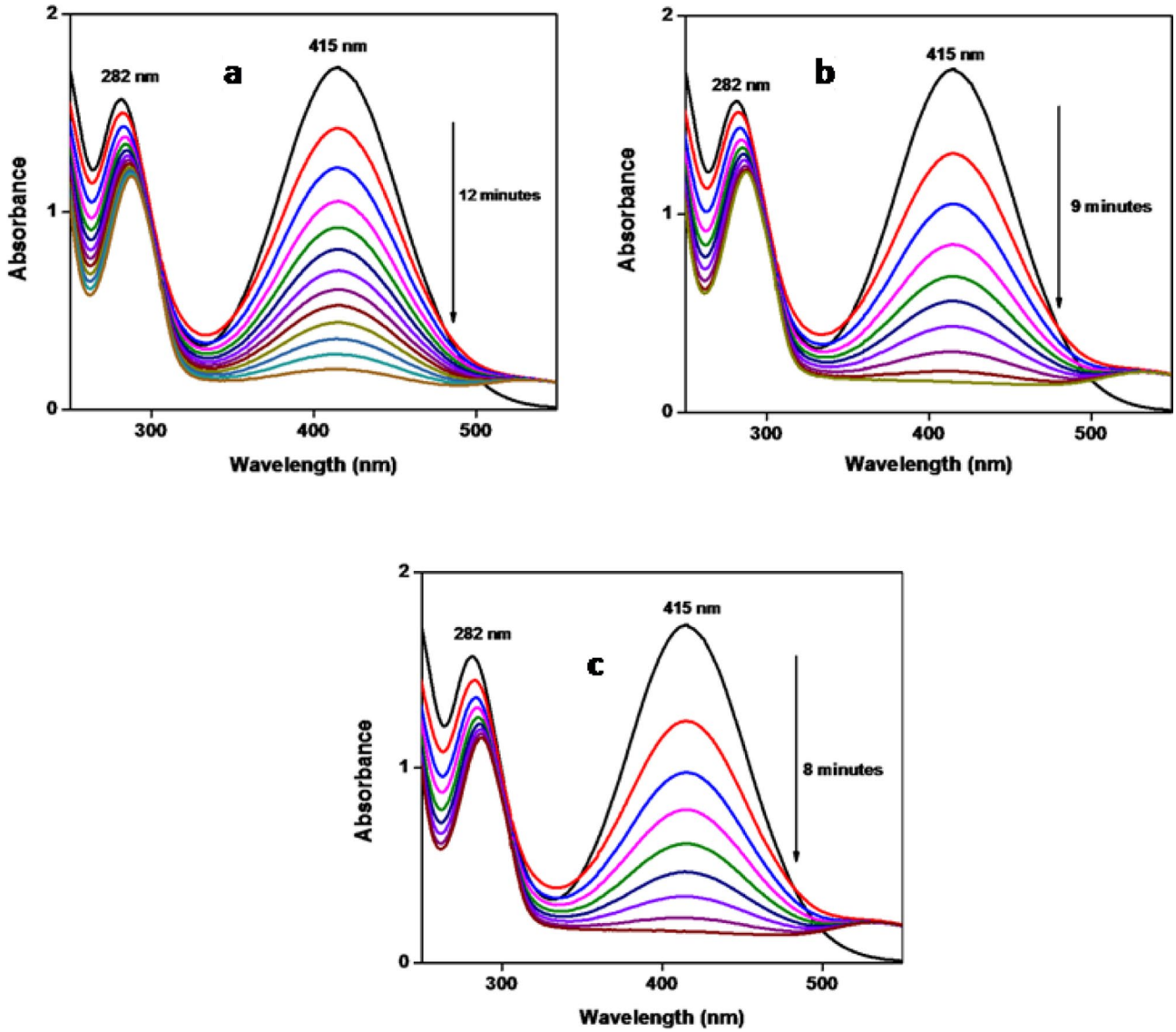

Fig. 13 UV–vis absorption spectra for the degradation of 2-nitrophenol by $NaBH_4$ in the presence of **a** 0.02, **b** 0.03, and **c** 0.04 mg/mL concentration of AuNP-AT catalyst

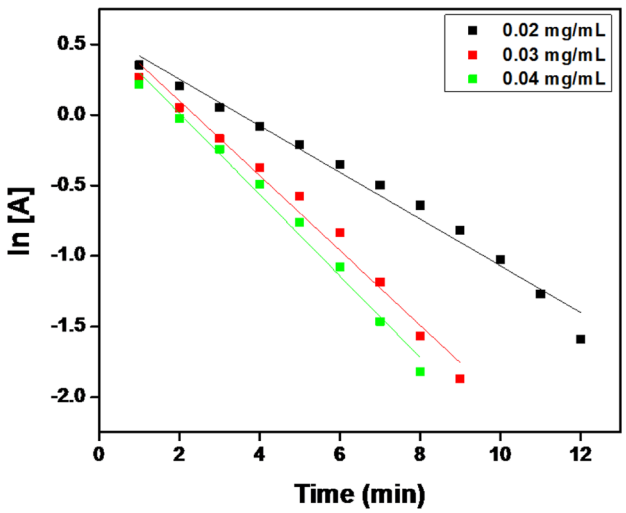

Fig. 14 Plot of *ln* [*A*] against time for the reduction of 2-nitrophenol

The kinetics of the reaction is studied by monitoring the changes in absorbance of the peak at 515 nm with time. As the concentration of $NaBH_4$ used in the degradation is much higher than that of the dye and AuNP-AT catalyst, it remains a constant throughout the reaction, and hence, it follows a pseudo-first-order kinetics. The reaction kinetics

Table 2 Catalytic activity of AuNP-AT in the reduction of 2-nitrophenol

Concentration of AuNP-AT ($mgmL^{-1}$)	Time (min)	Rate constant k (min^{-1})	Correlation coefficient (R^2)
0.02	12	0.1653	0.9798
0.03	9	0.2650	0.9822
0.04	8	0.2883	0.9872

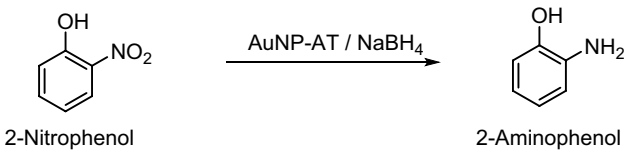

Fig. 15 Schematic representation for the reduction of 2-nitrophenol

is represented as $ln[A]/[A_0] = -kt$, where k is pseudo first order rate constant, $[A_0]$ is the concentration of eosin Y at time $t = 0$, and $[A]$ is the concentration at time "t." The value of $[A]$ is acquired from the absorbance value of the peak at 515 nm. The rate constant of the catalytic reduction can be directly obtained from the slope of ln $[A]$ versus time plot.

In order to study the effect of catalyst concentration on the rate of reduction, reactions were carried out using different concentrations of AuNP-AT catalyst, keeping all other parameters a constant. Straight line plots with good correlation coefficients were obtained in the ln $[A]$ versus time graph for all catalytic reactions (Fig. 10). A linear increase in the first-order rate constants with increase in concentration of the catalyst was also observed (Table 1). The schematic representation for the reduction of Eosin Y is shown in Fig. 11.

Catalytic Reduction of 2-Nitrophenol

Nitrophenols are a major class of toxic intermediates in the production of rubber chemicals, dyestuffs, pigments, and fungicides [38]. They are extensively used in laboratories as a good acid–base indicator. Nitrophenols are enlisted as priority pollutants by US-EPA due to their carcinogenic and mutagenic potential [39]. Decomposition of aqueous nitrophenol is very difficult even at low concentration. Therefore, their reduction into aminophenol is often appreciated due to its pharmaceutical importance of being an antecedent for the manufacture of various drugs [40].

The aqueous solution of 2-nitrophenol shows an absorption peak at 340 nm in UV–vis spectrum as shown in Fig. 12a. On the addition of $NaBH_4$, the characteristic peak at 340 nm shifted to 400 nm, due to the evolution of phenolate ions [41, 42]. Moreover, the pale yellow color of 2-nitrophenol changed to intense greenish yellow. The color of solution and peak intensity at 400 nm remains unaltered even after a long time of response. Although $NaBH_4$ exhibits its strong reducing power, only a very gradual reduction of 2-nitrophenol to 2-aminophenol can be attained by borohydride ions alone (Fig. 12b).

After the addition of a very small amount of AuNP-AT catalyst with increasing concentration, an enhanced rate of reduction was observed (Fig. 13). The reactions were portrayed by the regular diminishment of peak at 400 nm with time in the absorption spectrum and the peak at 282 nm was red-shifted to 290 nm. The emergence of a new peak around 290 nm and the drop of peak intensity at 400 nm correspond to the effectual reduction of 2-nitrophenol to 2-aminophenol by AuNP-AT catalyst [43]. As the concentration of $NaBH_4$ used was in excess, kinetics of the reduction follows pseudo-first-order with respect to 2-nitrophenol. Reaction kinetics was evaluated using the equation $ln[A]/[A_0] = -kt$, where k is the pseudo-first-order rate constant, and $[A]$ and $[A_0]$ are the concentrations of 2-nitrophenol corresponding to their absorbances at 400 nm on initial and "t" timings, respectively. Reaction constants were calculated from slopes of the linear plots of ln $[A]$ against time (Fig. 14).

The nanocatalyst facilitates the hydrogenation reaction by the coherent transfer of electrons from borohydride donor to nitrophenolate ion acceptor which was initiated upon the adsorption of both substrate ions onto the AuNP-AT catalyst surface. The electrons ejected to the metal surface from the

Table 3 Comparison of catalytic activity of AuNP-AT with various reported green synthesized nanoparticles

Dye	Type of nanoparticles	Plant extract	Rate constant (min^{-1})	Reference
Eosin Y	Silver	*Trigonella foenum-graecum*	0.2312	[44]
	Silver	*Hibiscus sabdariffa*	0.0282	[45]
	Gold	*Synedrella nodiflora*	0.1246	[46]
2-nitro phenol	Silver	*Caulis spatholobi*	0.1506	[47]
	Silver	*Duranta erecta*	0.0060	[48]
	Silver	*Cassia occiddentalis*	0.0244	[49]
	Copper	*Cassia occiddentalis*	0.0275	[49]
	Gold	*Caulis spatholobi*	0.1686	[47]
	Gold	*Amaranthus tricolor*	0.3377	This work
	Gold	*Amaranthus tricolor*	0.2883	This work

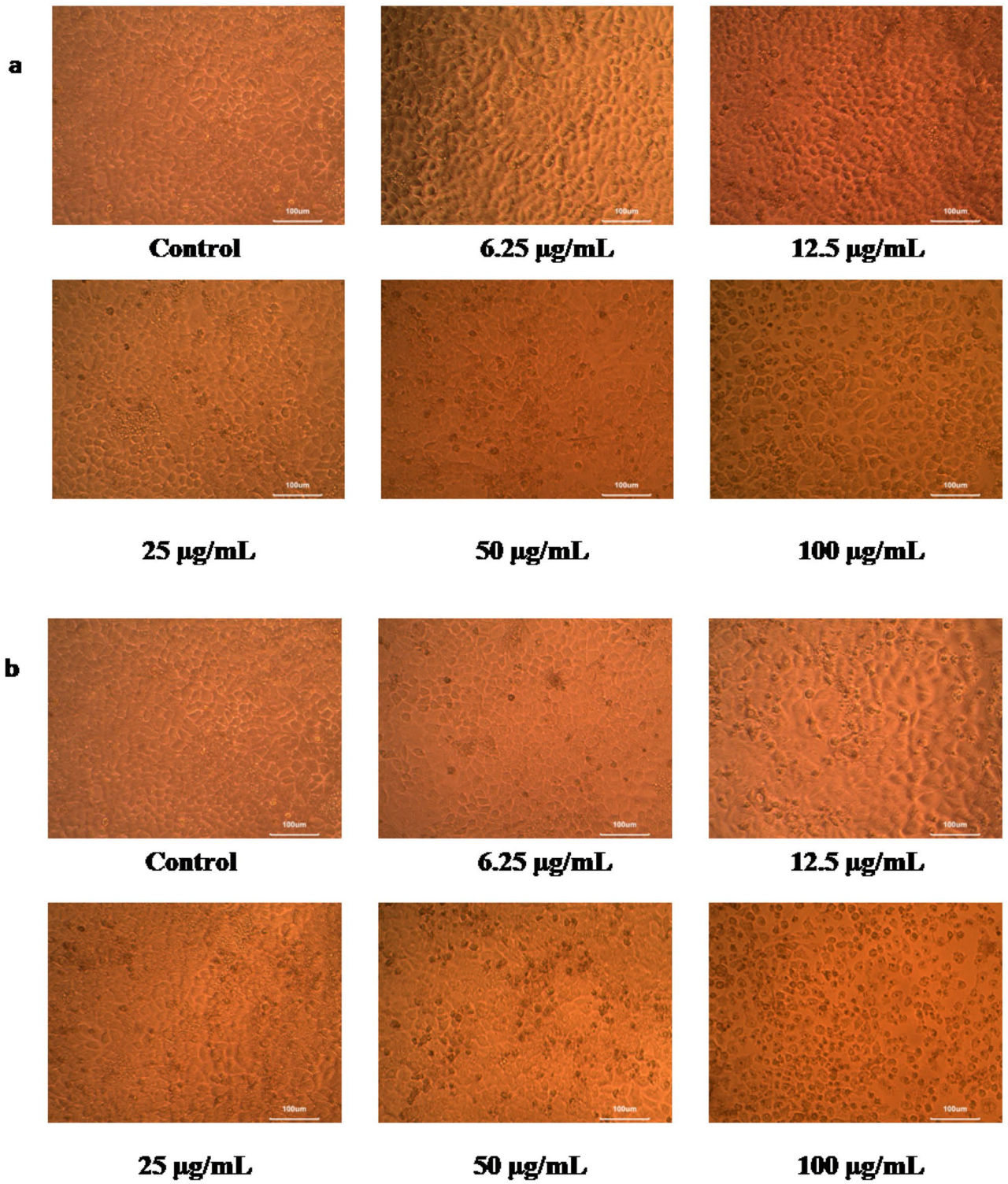

Fig. 16 Morphological changes induced on treated A549 cancer cell by **a** aqueous AT extract, and **b** AuNP-AT

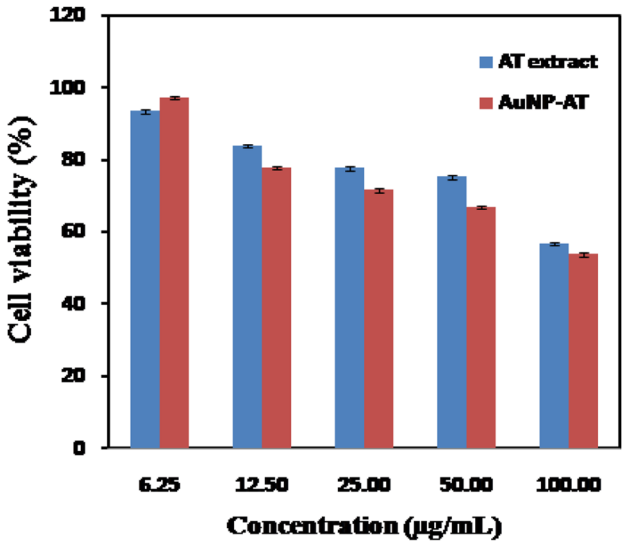

Fig. 17 The cell viability (%) of AT extract and AuNP-AT towards A549 cancer cell. Values are represented as the mean ± SD ($n = 3$)

borohydride ions are gained by phenolate ions and get easily reduced. To assess the dependence of catalyst concentration on the reaction, reductions were accomplished using different concentrations of AuNP-AT catalyst, keeping other parameters a constant. The first-order rate constants for the reactions using various concentrations of AuNP-AT catalyst with their respective correlation coefficients and time for degradation are shown in Table 2. Thus, the environmentally benign green gold nanoparticles act as a valid candidate for the productive use in waste water treatment. Figure 15 shows the schematic representation for the reduction of 2-nitrophenol. A comparison on the catalytic activity between AuNP-AT and various other green synthesized nanoparticles is shown in Table 3.

Cytotoxic Studies

The antiproliferative effect of aqueous AT leaf extract and AuNP-AT was investigated on human lung cancer cell line, A549 using MTT assay. Morphological changes including shrinking and granulation of the lung cancer cells caused by the interaction of AT extract and AuNP-AT are shown in Fig. 16a and b, respectively. Nanoparticles of gold penetrate into the cell membrane and associate with the proteins or nucleic acids and hence destroy the infected cells selectively [50]. The antiproliferative effect of nanoparticles is greatly attributed to its biocompatibility and high surface to volume ratio [51]. The presence of various bioactive components on the surface of nanoparticles is responsible for the generation of reactive oxygen species inside the cells which may also effectively contribute towards damaging of carcinoma cells. The LC_{50} values, concentration required for 50% cell death, were determined to be 118.851 ± 0.12 and 102.39 ± 0.36 µg/mL for AT extract and AuNP-AT, respectively, and were calculated using ED50 PLUS V1.0 software. The obtained results show that LC_{50} value is low for AuNP-AT than the AT extract itself. Figure 17 depicts the dose-dependent cell viability (%) induced by AT extract and AuNP-AT towards A549 cancer cells.

Antibacterial Studies

Antibacterial properties of the synthesized AuNP-AT nanoparticles were examined using agar diffusion well method against two gram negative bacteria: *Escherichia coli* and *Pseudomonas aeruginosa*; and two gram positive bacteria: *Streptococcus mutans* and *Staphylococcus aureus* as shown in Fig. 18. The antibacterial efficiency of AT extract and AuNP-AT is measured in terms of inhibition zone diameter (mm). The antibacterial activity of aqueous AT extract is attributed to the presence of alkaloids, tannins, flavanoids, saponins, proteins, and phenolic compounds in it. The synergetic effect from both nanosized gold and the bioactive phytoconstituents attached on its nanosurface contributed towards the higher antibacterial efficiency of the AuNP-AT particles. In case of gram negative bacteria: *Escherichia coli* and *Pseudomonasaeruginosa*, the zone of inhibition exhibited by the AuNP-AT is greater than that of AT extract. And the difference between their inhibition zones is much relevant. The close binding of nanoparticles with the phosphorus- and sulfur-containing components like DNA of the bacterial cell membrane leads to protein dysfunction and ultimate damage of the cell [52]. But in case of gram positive bacteria: *Streptococcus mutans* and *Staphylococcus aureus*, the zone of inhibition shown by the AuNP-AT is only slightly greater than that of AT extract. The very thin peptidoglycan layer present on the cell wall of gram negative bacteria permits the easy penetration of AuNP-AT into the bacterial cell and disturbs proper functioning of the cells by hindering the normal respiration and permeability [53]. While the presence of very thick peptidoglycan layers of the cell wall hinders the easy penetration of nanoparticles into the gram positive pathogens. Thus, the antibacterial efficiency of AuNP-AT is more significant in case of gram negative pathogens than the positive ones (Table 4).

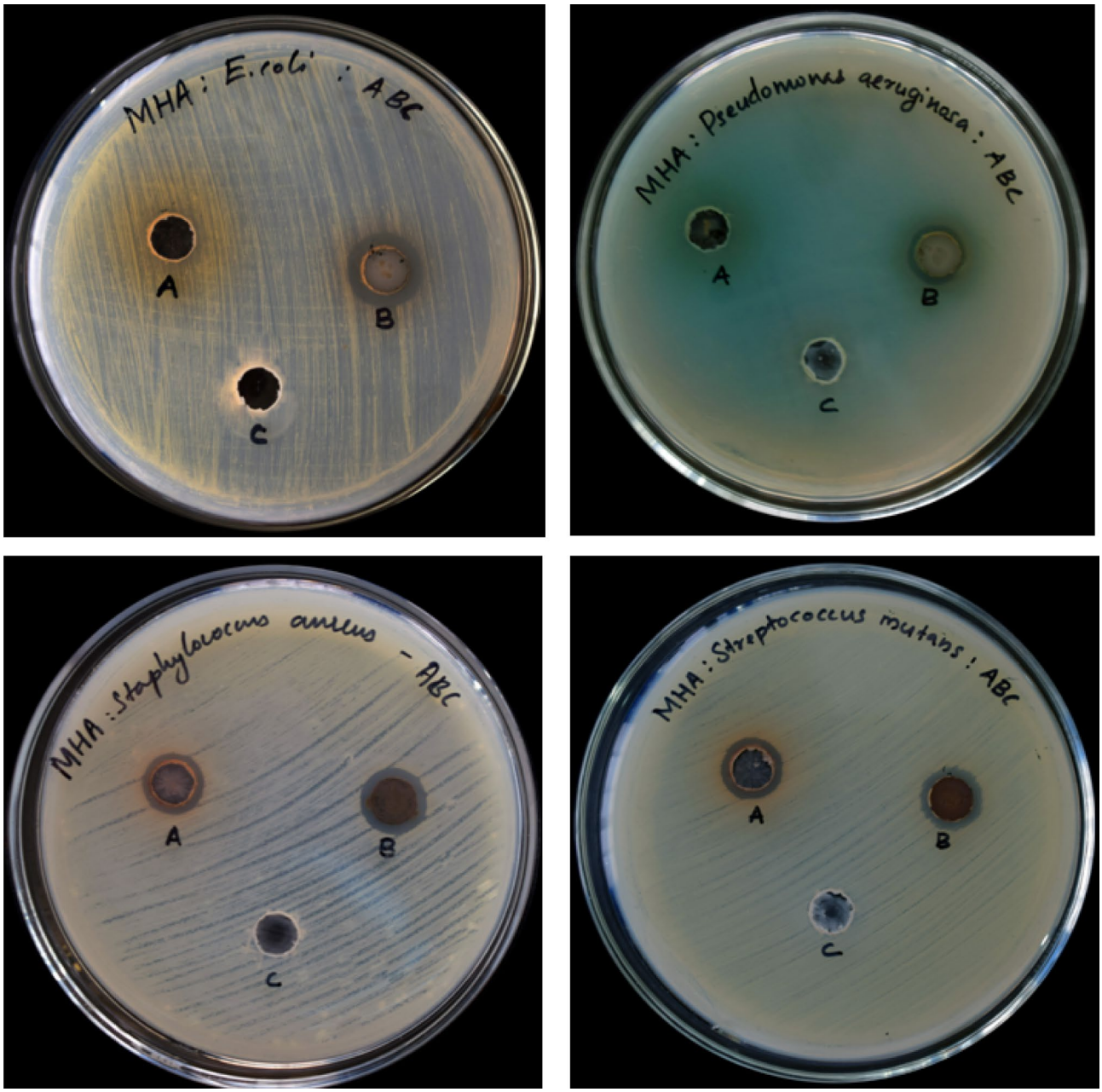

Fig. 18 Illustration of the antibacterial activity of AuNP-AT against *E. coli*, *P. aeruginosa*, *S. aureus*, and *S. mutans* using agar well diffusion method. [A: AT extract, B: AuNP-AT and C: control]

Table 4 Zone of inhibitions (mm) of AT extract, AuNP-AT, and control against various bacteria

Bacterial cultures	AT extract (mm)	AuNP-AT (mm)	Distilled water (mm)
E. coli	0	12.1 ± 0.23	0
P. aeruginosa	11.10 ± 0.47	14.9 ± 0.10	0
S. aureus	11.13 ± 0.15	12.1 ± 0.17	0
S. mutans	11.06 ± 0.40	11.2 ± 0.20	0

Conclusions

Microwave-assisted green synthesis of highly crystalline stable gold nanoparticles using the aqueous extract of *Amaranthus tricolor* leaves as both reducing and stabilizing agent is established. This is a simple, rapid, and eco-friendly method for the synthesis of noble metal gold nanoparticles. The synthesis of gold nanoparticles was optimized and the formed AuNP-AT were characterized by UV–vis., FT-IR, XRD, HR-TEM, EDX, DLS, and zeta potential measurements. The

prepared metal nanoparticles exhibited catalytic properties in the degradation of eosin Y and 2-nitrophenol. Both the catalytic degradations followed pseudo-first-order kinetics model with good correlation coefficients and rate of the reaction increased linearly with increasing catalytic dosage. The antiproliferative studies proved that the prepared nanoparticles can be used as a mighty weapon against human lung cancer cell lines, A549 and may be used in preparation of anticancer drug. The nanoparticles were found to be highly toxic towards various bacteria, which proved its antibacterial efficacy. This study emphasizes on the green synthetic protocols adopted for gold nanoparticles and their stupendous applications in the fields of catalysis and biomedicine.

Acknowledgements First author is grateful to University Grants Commission (UGC) for Senior Research Fellowship, and Department of Science & Technology (DST), Government of India for instrumentation facilities provided by DST-PURSE Phase II.

Author Contribution Mamatha Susan Punnoose: conceptualization, methodology, resources, data curation, writing — original draft; Siby Joseph: data curation, visualization; Bony K. John: data curation, visualization; Anu Rose Chacko: data curation, visualization; Sneha Mathew: data curation, visualization; Beena Mathew: conceptualization, supervision, project administration, writing — review & editing.

Data Availability All data generated or analyzed during this study are included in this manuscript.

Code Availability Not applicable.

Declarations

Ethics Approval Not applicable.

Consent to Participate All authors agree to participate in this investigation.

Consent for Publication All authors agree to participate in this article.

Conflict of Interest The authors declare no competing interests.

References

1. Reddy GB, Ramakrishna D, Madhusudhan A, Ayodhya D, Venkatesham M, Veerabhadram G (2015) Catalytic reduction of p-nitrophenol and hexacyanoferrate (III) by borohydride using green synthesized gold nanoparticles. J Chin Chem Soc 62(5):420–428
2. Deng HH, Li GW, Liu AL, Chen W, Lin XH, Xia XH (2014) Thermally treated bare gold nanoparticles for colorimetric sensing of copper ions. Microchim Acta 181(9):911–916
3. Cuenca AG, Jiang H, Hochwald SN, Delano M, Cance WG, Grobmyer SR (2006) Emerging implications of nanotechnology on cancer diagnostics and therapeutics. Cancer 107(3):459–466
4. Rodriguez P, Garcia-Araez N, Koverga A, Frank S, Koper MTM (2010) CO electroxidation on gold in alkaline media: A combined electrochemical, spectroscopic, and DFT study. Langmuir 26(14):12425–12432
5. Han J, Liu Y, Guo R (2009) Facile synthesis of highly stable gold nanoparticles and their unexpected excellent catalytic activity for Suzuki−Miyaura cross-coupling reaction in water. J Amer Chem Soc 131(6):2060–2061
6. Hayashi T, Tanaka K, Haruta M (1998) Selective Vapor-Phase Epoxidation of Propylene over Au/TiO_2 catalysts in the presence of oxygen and hydrogen. J Catal 178(2):566–575
7. Ghosh SK, Kundu S, Mandal M, Pal T (2002) Silver and gold nanocluster catalyzed reduction of methylene blue by arsine in a micellar medium. Langmuir 18(23):8756–8760
8. Pastoriza-Santos I, Liz-Marzán LM (2002) Formation of PVP-protected metal nanoparticles in DMF. Langmuir 18(7):2888–2894
9. Jiang H, Moon K, Zhang Z, Pothukuchi S, Wong CP (2006) Variable frequency microwave synthesis of silver nanoparticles. J Nanopart Res 8(1):117–124
10. Kundu S, Mandal M, Ghosh SK, Pal T (2004) Photochemical deposition of SERS active silver nanoparticles on silica gel and their application as catalysts for the reduction of aromatic nitro compounds. J Colloid Interface Sci 272(1):134–144
11. Majumdar R, Bag BG, Maity N (2013) *Acacia nilotica* (Babool) leaf extract mediated size-controlled rapid synthesis of gold nanoparticles and study of its catalytic activity. Int Nano Lett 3(1):1–6
12. Joseph S, Mathew B (2015) Microwave-assisted facile green synthesis of silver nanoparticles and spectroscopic investigation of the catalytic activity. Bull Mater Sci 38(3):659–666
13. Nadagouda MN, Speth TF, Varma RS (2011) Microwave-assisted green synthesis of silver nanostructures. Acc Chem Res 44(7):469–478
14. Punnoose MS, Mathew B (2002) Microwave-assisted green synthesis of Cyanthillium cinereum mediated gold nanoparticles: Evaluation of its antibacterial, anticancer and catalytic degradation efficacy. Res Chem Intermed 1:1–20
15. Punnoose MS, Bijimol D, Mathew B (2021) Microwave assisted green synthesis of gold nanoparticles for catalytic degradation of environmental pollutants. Environ Nanotechnol Monit Manag 16:100525
16. Lunardi CN, Barros MPF, Rodrigues ML, Gomes AJ (2018) Synthesis of gold nanoparticles using *Euphorbia tirucalli* latex and the microwave method. Gold Bull 51(4):131–137
17. Joseph S, Mathew B (2015) Microwave assisted facile green synthesis of silver and gold nanocatalysts using the leaf extract of *Aerva lanata*. Spectrochim Acta A Mol Biomol Spectrosc 136:1371–1379
18. Akintelu SA, Yao B, Folorunso AS (2021) Green synthesis, characterization, and antibacterial investigation of synthesized gold nanoparticles (AuNPs) from *Garcinia kola* pulp extract. Plasmonics 16(1):157–165
19. Cooper P (1993) Removing colour from bin dye house wastewater: a critical review of technology available. J Soc Dyers Colour 109(3):97–100
20. Yu K, Yang S, Liu C, Chen H, Li H, Sun C, Boyd SA (2012) Degradation of organic dyes via bismuth silver oxide initiated direct oxidation coupled with sodium bismuthate based visible light photocatalysis. Environ Sci Technol 46(13):7318–7326
21. Srivastava S, Sinha R, Roy D (2004) Toxicological effects of malachite green. Aquat Toxicol 66(3):319–329
22. Nemanashi M, Meijboom R (2013) Synthesis and characterization of Cu, Ag and Au dendrimer-encapsulated nanoparticles and their application in the reduction of 4-nitrophenol to 4-aminophenol. J Colloid Interface Sci 389(1):260–267
23. Vellaichamy B, Periakaruppan P (2016) A facile, one-pot and eco-friendly synthesis of gold/silver nanobimetallics smartened rGO for enhanced catalytic reduction of hexavalent chromium. RSC Adv 6(62):57380–57388

24. Faisal M, Abu Tariq M, Muneer M (2007) Photocatalysed degradation of two selected dyes in UV-irradiated aqueous suspensions of titania. Dyes Pigm 72(2):233–239
25. Rajan A, Vilas V, Philip D (2015) Catalytic and antioxidant properties of biogenic silver nanoparticles synthesized using Areca catechu nut. J Mol Liq 207(1):231–236
26. Tharun KNR, Padhy SK, Dinakaran SK, Banji D, Avasarala H, Ghosh S, Prasad MS (2012) Pharmacognostic, phytochemical, antimicrobial and antioxidant activity evaluation of *Amaranthus tricolor* Linn. Leaf Asian J Chem 24(1):455–460
27. Piattelli M, Giudici De Nicola M, Castrogiovanni V (1969) Photocontrol of amaranthin synthesis in *Amaranthus tricolor*. Phytochem 8(4):731–736
28. Aneja S, Vats M, Aggarwal S, Sardana S (2013) Phytochemistry and hepatoprotective activity of aqueous extract of Amaranthus tricolor Linn. Roots J Ayurveda and Integr Med 4(4):211
29. Bindhu MR, Umadevi M (2014) Surface plasmon resonance optical sensor and antibacterial activities of biosynthesized silver nanoparticles. Spectrochim Acta A Mol Biomol Spectrosc 121:596–604
30. Das J, Velusamy P (2014) Catalytic reduction of methylene blue using biogenic gold nanoparticles from *Sesbania grandiflora L.* J Taiwan Inst Chem Eng 45(5):2280–2285
31. Das RK, Gogoi N, Babu PJ, Sharma P, Mahanta C, Bora U (2012) The synthesis of gold nanoparticles using *Amaranthus spinosus* leaf extract and study of their optical properties. Adv Mater Phys Chem 2(4):275–281
32. Reddy GB, Madhusudhan A, Ramakrishna D, Ayodhya D, Venkatesham M, Veerabhadram G (2015) Green chemistry approach for the synthesis of gold nanoparticles with gum kondagogu: characterization, catalytic and antibacterial activity. J Nanostructure Chem 5(2):185–193
33. Vignesh K, Priyanka R, Hariharan R, Rajarajan M, Suganthi A (2014) Fabrication of CdS and $CuWO_4$ modified TiO_2 nanoparticles and its photocatalytic activity under visible light irradiation. J Ind Eng Chem 20(2):435–443
34. Wang F, Shao M, Cheng L, Chen D, Fu Y, Ma DDD (2009) Si/Pd nanostructure with high catalytic activity in degradation of eosin Y. Mater Res Bull 44(1):126–129
35. Kositzi M, Antoniadis A, Poulios I, Kiridis I, Malato S (2004) Solar photocatalytic treatment of simulated dyestuff effluents. Sol Energy 77(5):591–600
36. Lucas MS, Peres JA (2006) Decolorization of the azo dye Reactive Black 5 by Fenton and photo-Fenton oxidation. Dyes Pigm 71(3):236–244
37. Ghosh SK, Kundu S, Mandal M, Pal T (2022) Silver and gold nanocluster catalyzed reduction of methylene blue by arsine in micellar medium. Langmuir 18(23):8756–8760
38. Albukhari SM, Ismail M, Akhtar K, Danish EY (2019) Catalytic reduction of nitrophenols and dyes using silver nanoparticles @ cellulose polymer paper for the resolution of waste water treatment challenges. Colloids Surf A Physicochem 577(1):548–561
39. Keith L, Telliard W (1979) ES&T Special Report: Priority pollutants: I-a perspective view. Environ Sci Technol 13(4):416–423
40. Saha S, Pal A, Kundu S, Basu S, Pal T (2010) Photochemical green synthesis of calcium-alginate-stabilized Ag and Au nanoparticles and their catalytic application to 4-nitrophenol reduction. Langmuir 26(4):2885–2893
41. Junejo Y, Karaoğlu E, Baykal A (2013) Sirajuddin Cefditorene-mediated synthesis of silver nanoparticles and its catalytic activity. J Inorg Organomet Polym Mater 23(4):970–975
42. Ji T, Chen L, Schmitz M, Bao FS, Zhu J (2015) Hierarchical macrotube/mesopore carbon decorated with mono-dispersed Ag nanoparticles as a highly active catalyst. Green Chem 17(4):2515–2523
43. Kamal T, Khan SB, Asiri AM (2016) Nickel nanoparticles-chitosan composite coated cellulose filter paper: An efficient and easily recoverable dip-catalyst for pollutants degradation. Environ Pollut 218(1):625–633
44. Vidhu VK, Philip D (2014) Catalytic degradation of organic dyes using biosynthesized silver nanoparticles. Micron 56(1):54–62
45. Goswami M, Baruah D, Das AM (2018) Green synthesis of silver nanoparticles supported on cellulose and their catalytic application in the scavenging of organic dyes. New J Chem 42(13):10868–10878
46. Vijayan R, Joseph S, Mathew B (2018) Eco-friendly synthesis of silver and gold nanoparticles with enhanced antimicrobial, antioxidant, and catalytic activities. IET Nanobiotechnol 12(6):850–856
47. Le VT, Nguyen VC, Cao XT, Chau TP, Nguyen TD, Nguyen TLH (2021) Doan VD (2021) Highly effective degradation of nitrophenols by biometal nanoparticles synthesized using *Caulis Spatholobi* extract. J Nanomater 1:1–11
48. Albukhari SM, Ismail M, Akhtar K, Danish EY (2019) Catalytic reduction of nitrophenols and dyes using silver nanoparticles @ cellulose polymer paper for the resolution of waste water treatment challenges. Colloid Surf A-Physicochem Eng Asp 577(1):548–561
49. Gondwal M, Joshi nee Pant G (2018) Synthesis and catalytic and biological activities of silver and copper nanoparticles using *Cassia occidentalis*. Inter J Biomater 1:1–10
50. Fang J, Yu L, Gao P, Cai Y, Wei Y (2010) Detection of protein–DNA interaction and regulation using gold nanoparticles. Anal Biochem 399(1):262–267
51. Cui W, Li J, Zhang Y, Rong H, Lu W, Jiang L (2010) Effects of aggregation and the surface properties of gold nanoparticles on cytotoxicity and cell growth. Nanomedicine 8(1):46–53
52. Soshnikova V, Kim YJ, Singh P, Huo Y, Markus J, Ahn S, Castro-Aceituno V, Kang J, Chokkalingam M, Mathiyalagan R, Yang DC (2018) Cardamom fruits as a green resource for facile synthesis of gold and silver nanoparticles and their biological applications. Artif Cells Nanomed Biotechnol 46(1):108–117
53. Rajan A, Vilas V, Philip D (2015) Studies on catalytic, antioxidant, antibacterial and anticancer activities of biogenic gold nanoparticles. J Mol Liq 212(1):331–339